Refined Calculation of the Phase Separation Behavior of Sheared Polymer Blends: Closed Miscibility Gaps within Two Ranges of Shear Rates

R. Horst and B. A. Wolf*

Institut für Physikalische Chemie der Universität Mainz, Jakob-Welder-Weg 13, D-55099 Mainz, Germany

*Received March 5, 1993; Revised Manuscript Received July 23, 1993**

ABSTRACT: The phase diagrams of a blend of two homopolymers exhibiting a lower critical solution temperature (LCST) have been calculated on the basis of the generalized Gibbs energy of mixing (sum of the Gibbs energy of mixing of the stagnant blend and the energy the mixture can store during stationary flow) for various shear rates $\dot{\gamma}$. In the present paper the temperature dependence of the energy stored in blends was taken into account. The calculations yield a complex dependence: With increasing $\dot{\gamma}$ the heterogeneous region of the phase diagram is first reduced (shear dissolution), then enlarged (shear demixing), and finally reduced again. So, with varying $\dot{\gamma}$, the influences of shear change sign twice; i.e., two inversions of the effects are observed. For very high $\dot{\gamma}$ values the system behaves like in the quiescent state. Closed miscibility gaps can occur within two ranges of $\dot{\gamma}$: Within the first range the islands show up below T_c (the critical temperature of the system) and merge into the original miscibility gap as $\dot{\gamma}$ is raised; the first inversion point is located in this area. The second $\dot{\gamma}$ range of islands (entirely located above T_c) is observed within the regime of the second shear dissolution. The occurrence of islands can be suppressed for an appropriate choice of parameters and the previously published simpler behavior is regained.

Introduction

The phase separation behavior of polymer-containing systems is markedly changed by flow,[1-21] especially in the case of polymer blends. But measurements reported in the literature do not seem to be consistent. All effects one can think of are reported; this is even true for the blend polystyrene/poly(vinyl methyl ether) which is most frequently investigated.[22] One can therefore conclude that the influence of shear on the phase diagrams of polymer blends is a complex one. Consequently, it appeared interesting to investigate this behavior with the theoretical approach[23] that has already been very successful in describing the multitude of phenomena observed for polymer solutions.[24,25] As will be demonstrated, it is possible to reconcile the seemingly contradicting experimental results reported in the literature by these theoretical calculations.

The basis of the present approach is the generalized Gibbs energy of mixing[23] for flowing systems; it is given as the sum of the Gibbs energy of the stagnant mixture and the energy the system can store during flow. An elaboration of this approach in terms of phenomenological thermodynamics has been recently reported.[26] In one of the preceding papers[24] we calculated the phase diagrams of sheared polymer *solutions*, treating the stored energy temperature dependent. In that publication we predicted a new phenomenon in the case of LCSTs, namely, the occurrence of a closed miscibility gap in the homogeneous region of the phase diagram of the quiescent system. In another paper[25] we dealt with the shear influence on phase diagrams of polymer *blends*. But for these calculations it was for simplicity assumed that the stored energy is constant within the small temperature interval of interest. On this basis one obtains a shift in the demixing temperature (LCST) that is positive at the lowest shear rates; i.e., the homogeneous area is enlarged (For short, this phenomenon is called shear dissolution.). At the highest shear rates one also finds shear dissolution, but for an intermediate $\dot{\gamma}$ range the demixing temperature is lowered; i.e., the heterogeneous area is enlarged (shear demixing). This means that the effect of shear on the demixing temperature changes two times its sign as the shear rate is varied.

Some experimentally observed features of shear influences can already be well described by the results of the above theoretical calculations. For instance, the second inversion has already been observed experimentally for a blend of poly(ethylene-*co*-vinyl acetate)/solution-chlorinated polyethylene.[21] Another finding that is qualitatively explained is the occurrence of island curves.[24] Higgins and Fernandez[27] carried out experiments with the system PS/PVME. Their results are in good agreement with our prediction; there are however also some differences.

To cover all experimentally observed phenomena we have improved our theoretical ansatz for polymer blends so that it now accounts for the temperature dependence of the viscosity, i.e., treats the stored energy temperature dependent.

Theoretical Treatment of Flowing Systems

All equations used in the following calculations are identical with those of the preceding paper except for eq 18, which describes the temperature dependence of the viscosity. For this reason the equations are only shortly presented; more details can be found in the preceding publication.[25]

The coexistent phases of a binary system are given by the conditions (eqs 1 and 2) that the chemical potentials μ of each component, indicated by the index A or B, are equal in the two phases, indicated by a single prime or two primes.

$$\mu_A' = \mu_A'' \tag{1}$$

$$\mu_B' = \mu_B'' \tag{2}$$

In a flowing system the Gibbs energy of mixing has to be modified, because the system can store energy during flow.[23] This stored energy E_s is accumulated until the steady state is reached at the given shear rate and is

* Abstract published in *Advance ACS Abstracts*, September 15, 1993.

0024-9297/93/2226-5676$04.00/0

released when the shear stress stops and the system relaxes to equilibrium.

A generalized Gibbs energy of mixing G_γ was therefore introduced[23] by adding E_s to G_z, the Gibbs energy at zero shear.

$$G_\gamma = G_z + E_s \tag{3}$$

The coexistence conditions then become in terms of the mole fraction x

$$\mu_A' + \left(E_s' - \left(\frac{\partial E_s}{\partial x_B}\right)' x_B'\right) = \mu_A'' + \left(E_s'' - \left(\frac{\partial E_s}{\partial x_B}\right)'' x_B''\right) \tag{4}$$

$$\mu_B' + \left(E_s' + \left(\frac{\partial E_s}{\partial x_B}\right)'(1 - x_B')\right) = \mu_B'' + \left(E_s'' + \left(\frac{\partial E_s}{\partial x_B}\right)''(1 - x_B'')\right) \tag{5}$$

How these two summands of G_γ can be evaluated in the case of mixtures of two polymers is the subject of the next section.

Modeling of Polymer Blends

Gibbs Energy of Mixing of the Stagnant System. The chemical potentials of the two polymers of a blend can be represented by the Flory–Huggins equation

$$\frac{\Delta\mu_A}{N_A RT} = \frac{1}{N_A}\ln\varphi_A + \left(\frac{1}{N_A} - \frac{1}{N_B}\right)\varphi_B + g\varphi_B^2 \tag{6}$$

$$\frac{\Delta\mu_B}{N_B RT} = \frac{1}{N_B}\ln\varphi_B + \left(\frac{1}{N_B} - \frac{1}{N_A}\right)\varphi_A + g\varphi_A^2 \tag{7}$$

where φ stands for volume fractions and N is the number of segments of the polymer, calculated by division of the molar volumes V_A and V_B, respectively, by the molar volume V_s of a segment. The molar volumes of the polymers are accessible from their masses M and densities ρ; the value of V_s can be freely chosen and is normally selected in the range of the monomeric units of the polymers. The Flory–Huggins interaction parameter g under the critical conditions is given by

$$g_c = \frac{1}{2}\left(\frac{1}{N_A^{1/2}} + \frac{1}{N_B^{1/2}}\right)^2 \tag{8}$$

The temperature dependence of g can in the small temperature interval of interest be represented as

$$g = g_c + g_1(T - T_c) \tag{9}$$

Stored Energy. E_s is accessible from the average molar volume of the blend, the steady-state shear compliance $J_e°$, the viscosity η, and the shear rate $\dot\gamma$ according to

$$E_s = (x_A V_A + x_B V_B)\langle J_e°\rangle(\langle\eta\rangle\dot\gamma)^2|\langle\eta\rangle\dot\gamma|^{-2d^*} \tag{10}$$

The shear rate dependence of the viscosity can be described by Graessley's[28] equation (eqs 11–14); η_0 is the zero shear viscosity, and τ_0 is the characteristic viscometric relaxation time.

$$\langle\eta\rangle/\langle\eta_0\rangle = g^{1.5}(\theta)\, h(\theta) \tag{11}$$

$$\theta = \frac{\langle\eta\rangle}{\langle\eta_0\rangle}\frac{\dot\gamma\langle\tau_0\rangle}{2} \tag{12}$$

Table I. Parameters Needed for the Calculation of the Phase Diagrams[a]

parameter	value	parameter	value
T_c (K)	400	V_s (m³/mol)	10^{-4}
g_1 (K⁻¹)	3×10^{-6}	ρ (kg/m³)	1000
K (Pa s)	10^{-3}	M_A (kg/mol)	75
E^* (kJ/mol)	25	M_B (kg/mol)	200

[a] Identical to those of ref 25, except for g_1 (modified) and E^* (new).

$$g(\theta) = \frac{2}{\pi}\left(\operatorname{arccot}\theta + \frac{\theta}{1+\theta^2}\right) \tag{13}$$

$$h(\theta) = \frac{2}{\pi}\left(\operatorname{arccot}\theta + \frac{\theta(1-\theta^2)}{(1+\theta^2)^2}\right) \tag{14}$$

The negative slope of the flow curve, d^*, defined by

$$d^* = -\left(\frac{\partial\ln\eta}{\partial\ln\dot\gamma}\right) \tag{15}$$

can be calculated by eqs 11–14.

$J_e°$ and τ_0 are interrelated by

$$J_e° = \tau_0/\eta_0 \tag{16}$$

where τ_0 can be set equal to the Rouse[29] relaxation time τ_R

$$\tau_0 = \tau_R = \frac{6}{\pi^2}\frac{\eta_0 M}{\rho RT} \tag{17}$$

The temperature dependence of η_0 is introduced via the Arrhenius equation (eq 18), in which E^* is the activation energy, taking the critical temperature T_c as the reference temperature.

$$\eta_0 = \eta_0(T_c)\exp\left(\frac{E^*}{R}\left(\frac{1}{T} - \frac{1}{T_c}\right)\right) \tag{18}$$

calculating η_0 at T_c by means of

$$\eta_0(T_c) = K(M/(\text{kg mol}^{-1}))^{3.4} \tag{19}$$

The zero shear viscosity and the steady-state shear compliance of the mixture can be calculated by eqs 20 and 21 from the values of the pure components[30] using the weight fractions w.

$$\langle\eta_0\rangle 1/3.4 = w_A\langle\eta_A\rangle^{1/3.4} + w_B\langle\eta_B\rangle^{1/3.4} \tag{20}$$

$$\langle J_e°\rangle = \frac{w_A\eta_{0A}^{4.4/3.4}J_{eA}° + w_B\eta_{0B}^{4.4/3.4}J_{eB}°}{\langle\eta_0\rangle^{4.4/3.4}} \tag{21}$$

All equations needed are introduced and phase diagrams can be calculated for flowing blends. The set of parameters used for the present modeling is given in the next section.

Choice of Parameters

The parameters of the subsequent calculations are identical with those used in the preceding paper[25] except for the newly introduced E^* and a smaller g_1 value; again $\rho_A = \rho_B = \rho$ and $K_A = K_B = K$. All data are collected in Table I.

With the parameters given in Table I one first calculates the stored energy for a given shear rate by means of eqs 10–21. As an example the curves for a shear rate of 0.2 s^{-1} are given in Figure 1.

As can be seen in Figure 1, there are three temperature ranges of different curvature of $E_s(x_B)$. From the highest temperatures down to 410 K the curvature of $E_s(x_B)$ is positive. This means that shear dissolution is to be expected in this area. Below 400 K there is a hump so that

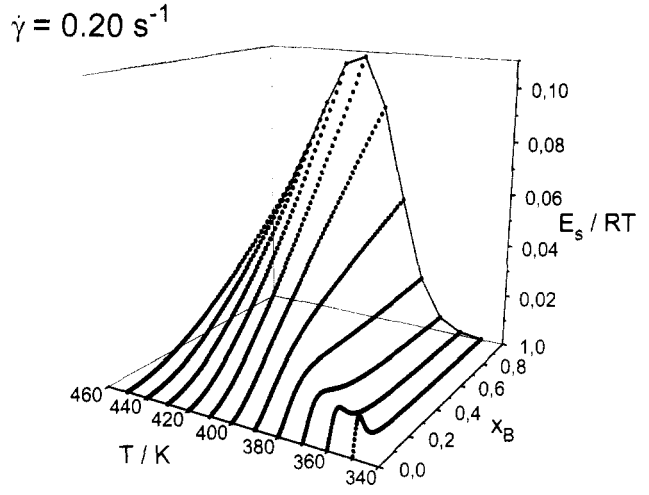

Figure 1. Reduced stored energy E_s/RT as a function of x_B, the mole fraction of component B, and the temperature T. The data points for the pure component B are connected by a line.

the curvature is negative within a great composition range; i.e., shear demixing is favored. As the temperature is lowered further, this hump becomes smaller and shifts toward higher A contents. This results in shear dissolving behavior at temperatures below 370 K.

These features of E_s, visible from Figure 1, can be explained in terms of the disentanglement processes which are enhanced by higher shear rates and lower temperatures (longer relaxation times). At the high temperatures the relaxation time is so small, even for the high molecular mass component B, that the mixture behaves Newtonian in the entire composition range. Therefore η increases monotonously with the content of B and so does E_s. This explains the positive curvature in this temperature range. Reduction of T leads to an augmentation of τ_0. Hence the disentanglement process starts in mixtures rich in B at a certain T where mixtures rich in A still behave Newtonian. Therefore a hump in E_s, which results in a shear demixing, is generated. For even lower temperatures, τ_0 becomes so large for both components that also mixtures rich in A behave non-Newtonian. The hump in E_s is then shifted to the A side (lower molecular mass component), and shear dissolution is observed in the concentration range given by the equilibrium miscibility gap.

As the shear rate is raised, the "mountain" shown in Figure 1 becomes larger and shifts toward higher temperatures.

To solve the conditions (4) and (5) for the coexistence of two phases, the dependence of the stored energy on composition must be given as an analytical function. For fitting purposes we used eq 22, which is a linear function with a Lorentz peak put on; x_p is the position of the peak maximum, h is its height, and w is its width.

$$E_s = E_{sA} - h\frac{w^2}{w^2 + 4x_p^2} + x_B\left(E_{sB} - E_{sA} + h\left(\frac{w^2}{w^2 + 4x_p^2} - \frac{w^2}{w^2 + 4(1 - x_p)^2}\right)\right) + h\frac{w^2}{w^2 + 4(x_B - x_p^2)} \quad (22)$$

Combining the above relation with eqs 6–9, describing the equilibrium behavior, the phase diagrams of the sheared polymer blend can be calculated. This was done on an IBM AT personal computer with an algorithm written in TURBO-Pascal. The exact procedure is described in ref 24. The phase diagrams calculated with the parameters given in Table I are presented in the next section.

Results and Discussion

The tie lines at 400 K remain the same as in the preceding paper;[25] i.e., the inversion points must be identical, because of the same molecular masses of the polymers and the same parameters (g_1 and E^* have no influence on the behavior at the critical temperature). However, island curves must be obtained for appropriate parameters, since the temperature dependence of the stored energy is now taken into account. With our choice of parameters the closed miscibility gaps already calculated for polymer solutions appear at shear rates between 0.175 and 0.25 s^{-1} as can be seen from Figure 2.

In contrast to the previous calculations, the present yields a second $\dot{\gamma}$ range of closed miscibility gaps. These islands of immiscibility occur at $\dot{\gamma}$ values between 0.85 and 0.9 s^{-1} and at higher temperatures than the first ones (Figure 3).

Figure 4 gives all phase diagrams that have been calculated. At low and at high shear rates the heterogeneous area is reduced; in the intermediate $\dot{\gamma}$ range it is enlarged.

The present calculations yield phase diagrams that are in many aspects very similar to those computed for polymer blends in the preceding paper[25] under the neglection of the T dependence of E_s. In addition, however, they exhibit

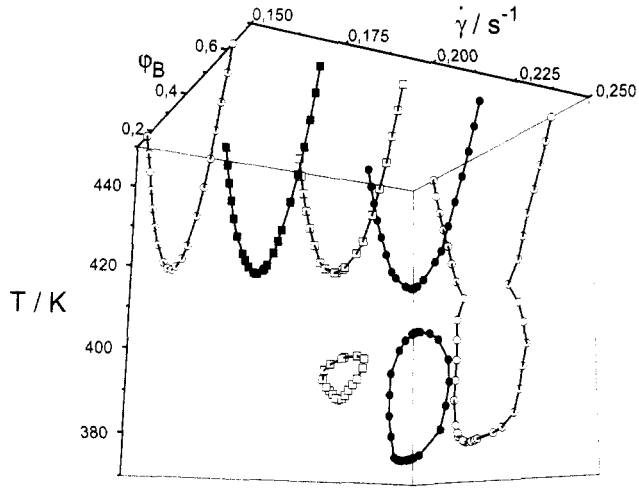

Figure 2. Phase diagrams for the model blend A75/B200 (the numbers give the molar masses in kg/mol) in the region of low shear rates $\dot{\gamma}$. The first $\dot{\gamma}$ range with closed miscibility gaps is shown.

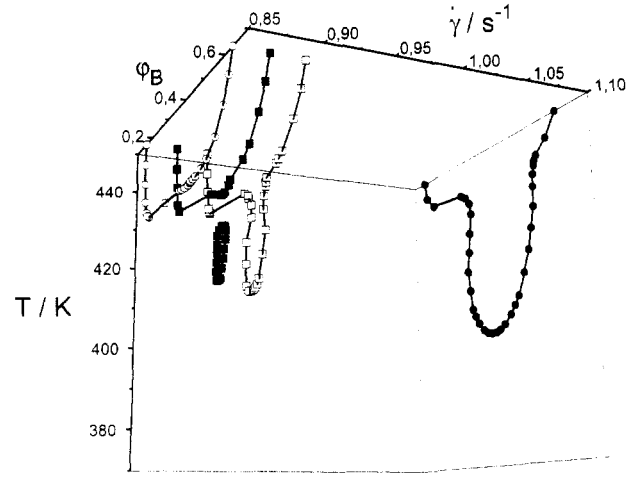

Figure 3. Phase diagrams at different shear rates $\dot{\gamma}$ for the model blend A75/B200. The second $\dot{\gamma}$ range with closed miscibility gaps is shown.

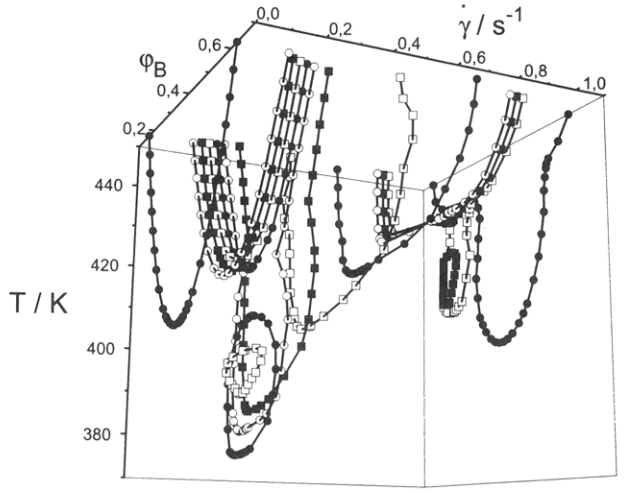

Figure 4. Phase diagrams at different shear rates $\dot{\gamma}$ for the model blend A75/B200. All diagrams that have been calculated are shown.

two peculiarities that can only be observed if one accounts for the changes in the rheological behavior of the system associated with the variation of the temperature.

The first extra effect is the occurrence of closed miscibility gaps at low shear rates. Their existence was foreseeable because of calculations concerning the shear influence on polymer *solutions*.[24] Their appearance can be explained by the above-described shape of E_s. At the presently discussed low shear rates, E_s acts toward shear dissolution in the temperature range of the equilibrium miscibility gap. But at lower temperatures E_s favors shear demixing. As $\dot{\gamma}$ is raised, this demixing range comes so close to the critical point that it induces phase separation and an island is created. These closed miscibility gaps are normally situated well below T_c and they are primarily caused by the stored energy.

In the case of the polymer *blends* the islands are much bigger and their shape is different. They no longer look like a banana as in the case of *solutions*, but they are circular and located in the same composition range as the equilibrium miscibility gap. Because the stored energy E_s is larger and G_z smaller, the island can lie in the composition–temperature range of the equilibrium miscibility gap; i.e., the upper end of the island is situated above T_c (cf. the island depicted by full circles at 0.225 s^{-1} in Figures 2 and 4). As the shear rate is raised, these islands are shifted toward higher temperatures and finally melt into the heterogeneous domain corresponding to the equilibrium miscibility gap.

Another new observation is the existence of closed miscibility gaps in a second, higher range of shear rates just before the shear influences fade away and the form of the equilibrium miscibility gap is restored (cf. the island depicted by full squares at 0.875 s^{-1} in Figures 3 and 4). This observation can be explained in the following manner: At temperatures which are considerably larger than critical, the stored energy favors the phase-separated state, as can be seen from the fact that the miscibility gap broadens under these conditions. Upon a reduction of T the influence of the stored energy changes sign and acts strongly toward homogenization; here it is large enough to overcompensate G_z such that the system becomes homogeneous in the whole composition range. As T is still lowered, the influence of E_s decreases so rapidly that the system demixes again and a closed miscibility gap is created. These islands are caused by G_z and can only be located within the equilibrium solubility gap.

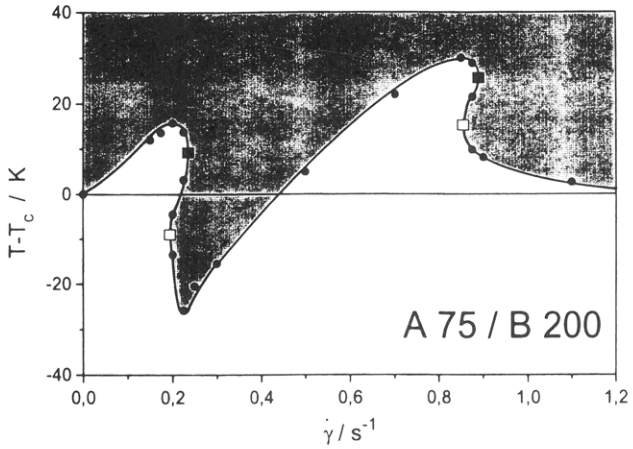

Figure 5. Projection of the heterogeneous regions (shaded area) onto the T–$\dot{\gamma}$ plane. $T - T_c$ is the difference to the critical temperature T_c (400 K), and $\dot{\gamma}$ is the shear rate. The open squares give the conditions at which the islands show up, and the full squares where they coalesce with the original miscibility gap.

A simplified representation of the results is given in Figure 5. It is obtained from Figure 4 by projection of the phase diagrams onto the T–$\dot{\gamma}$ plane. In Figure 5 the *curve of demixing* separates the areas of complete and incomplete miscibility (shaded part). One can distinguish between parts of the curve that correspond to the normal situation observed with LCSTs (entrance into the two-phase regime upon heating) and others for which the opposite is true (i.e., entrance upon cooling). The parts of the demixing curve that correspond to the former case are subsequently called the *line of normal demixing* and that corresponding to the latter case the *line of contrary demixing*.

Starting from zero shear, the homogeneous region is extended; i.e., the solubility gap shifts toward higher temperatures and shear dissolution takes place. At a certain $\dot{\gamma}$ an island emerges (first open square in Figure 5). With increasing $\dot{\gamma}$ the island grows and melts into the original two-phase area (first full square). The part of the demixing curve situated between these two points constitutes a line of contrary demixing. It corresponds to the high-temperature side of the island. Within the $\dot{\gamma}$ range given by these squares there also exist lines of normal demixing. The upper one corresponds to the minima of the original miscibility gaps and the lower one to the low-temperature side of the islands. In this range of shear rates three phase transitions can be observed upon the variation of T. For a starting point at high temperatures the system is heterogeneous. Temperature reduction homogenizes the mixture. Then the line of contrary demixing is passed and the system demixes; it is now in the region of the island. Upon further cooling the region of the closed miscibility gap is left and the system becomes one-phase again.

As one increases the shear rate beyond the point where the island coalesces with the main solubility gap, the situation becomes normal again and one observes just one phase transition for a given shear rate. The effect of shear demixing becomes smaller as $\dot{\gamma}$ is raised and after an inversion the system behaves shear-dissolving. This second range of shear dissolution can only be observed with polymer blends.[21,25]

Finally, at very high shear rates a second range of islands exists and one enters a second line of contrary demixing (located between the full and the open square). As discussed before, these second islands are all situated above T_c. Upon a still further augmentation of $\dot{\gamma}$ the shear influences fade away, and the system behaves as if it were at equilibrium.

At first glance the curve shown in Figure 5 seems to be very different from the one calculated in the preceding paper.[25] However, for a suitable choice of the parameters describing the temperature dependences of the stored energy (E^*) and the Flory–Huggins interaction parameter (g_1), the open and the full squares collapse at both island ranges, and the smooth behavior described in the preceding paper[25] is regained. The existence of islands is suppressed if the temperature dependence of the stored energy becomes small compared to that of the interaction parameter. For that reason, the previously published curve ($E^* = 0$ kJ/mol) is only a special case of behavior resulting from the present approach.

Conclusions

The shear influence on the phase behavior of polymer blends exhibiting LCSTs can be summarized as follows:

(i) Low shear rates induce a shift of the demixing temperature to higher values. The homogeneous area of the phase diagram is enlarged (shear dissolution).

(ii) At a certain characteristic $\dot{\gamma}$ value an island of immiscibility can occur (depending on the particular system-specific parameters of the blend of interest). The two-phase regions of these islands can be located below T_c, which means that phase separation is induced by shear (shear-demixing). Upon a further augmentation of $\dot{\gamma}$ its extension increases and finally it melts into the original miscibility gap at another, higher characteristic shear rate. In the $\dot{\gamma}$ range given by these two characteristic values it is possible to observe phase separation upon cooling as well as upon heating. It is also within the above-mentioned $\dot{\gamma}$ range that the effects of shear change sign for the first time, namely, from shear-dissolution to shear-demixing.

(iii) A further increase of the shear rate causes a second inversion, this time from shear-demixing to shear-dissolution.

(iv) A second zone of islands turns up at still higher shear rates. These closed solubility gaps are located above the critical temperature (minimum demixing temperature of the quiescent system). After the coalescence of the island with the main two-phase area, the shear effects fade away and the system behaves like in the quiescent state.

Acknowledgment. We are grateful to the Deutsche Forschungsgemeinschaft for the support of this work and to M. Fernandez and J. Higgins (Imperial College of Science, Technology and Medicine, London) for stimulating discussions.

References and Notes

(1) Breitenbach, J. W.; Wolf, B. A. *Makromol. Chem.* **1968**, *117*, 163.
(2) Ver Strate, G.; Philippoff, W. *J. Polym. Sci., Polym. Lett. Ed.* **1974**, *12*, 267.
(3) Torkelson, J. M.; Tirrell, M.; Frank, C. W. *Macromolecules* **1984**, *17*, 1505.
(4) Wölfle, A.; Springer, J. *Colloid Polym. Sci.* **1984**, *262*, 876.
(5) Hashimoto, T.; Takebe, T.; Suehiro, S. *Polym. J.* **1986**, *18*, 123.
(6) Onuki, Akira *Phys. Rev.* **1987**, *35*, 5149.
(7) Lyngaae-Jorgensen, J.; Sondergaard, K. *Polym. Eng. Sci.* **1987**, *27*, 351.
(8) Rector, L. P.; Mazich, K. A.; Carr, S. H. *J. Macromol. Sci., Phys.* **1988**, *B27*, 421.
(9) Bhattacharjee, S. M.; Fredrickson, G. H.; Helfand, E. *J. Chem. Phys.* **1989**, *90*, 3305.
(10) Nakatani, A. I.; Kim, H.; Takahashi, Y.; Han, C. C. *Polym. Commun.* **1989**, *30*, 143.
(11) Vshivkov, S. A.; Pastukhova, L. A.; Titov, R. V. *Polym. Sci. USSR (Engl. Transl.)* **1989**, *31*, 1541.
(12) Katsaros, J. D.; Malone, M. F.; Winter, H. H. *Polym. Eng. Sci.* **1989**, *29*, 1434.
(13) Takebe, T.; Sawaoka, R.; Hashimoto, T. *J. Chem. Phys.* **1989**, *91*, 4369.
(14) Barham, P. J.; Keller, A. *Macromolecules* **1990**, *23*, 303.
(15) Nakatani, A. I.; Kim, H.; Han, C. C. *J. Res. Natl. Bur. Stand.* **1990**, *95*, 7.
(16) Kammer, H. W.; Kummerloewe, C.; Kressler, J.; Melior, J. P. *Polymer* **1991**, *32*, 1488.
(17) Yanase, H.; Moldenaers, P.; Mewis, J.; Abetz, V.; van Egmond, J.; Fuller, G. G. *Rheol. Acta* **1991**, *30*, 89.
(18) Mani, S.; Malone, M. F.; Winter, H. H.; Halary, J. L.; Monnerie, L. *Macromolecules* **1991**, *24*, 5451.
(19) Laun, H. M.; Bung, R.; Hess, S.; Loose, W.; Hess, O.; Hahn, K.; Hädicke, E.; Hingmann, R.; Schmidt, F.; Lindner, P. *J. Rheol.* **1992**, *36*, 743.
(20) Douglas, J. F. *Macromolecules* **1992**, *25*, 1468.
(21) Hindawi, I. A.; Higgins, J. S.; Weiss, R. A. *Polymer* **1992**, *33*, 2522.
(22) Larson, R. G. *Rheol. Acta* **1992**, *31*, 497.
(23) Wolf, B. A. *Macromolecules* **1984**, *17*, 615.
(24) Horst, R.; Wolf, B. A. *Macromolecules* **1991**, *24*, 2236.
(25) Horst, R.; Wolf, B. A. *Macromolecules* **1992**, *25*, 5291.
(26) Criado-Sancho, M.; Jou, D.; Casas-Vázquez, J. *Macromolecules* **1991**, *24*, 2834.
(27) Fernandez, M.; Higgins, J., Private communication.
(28) Graessley, W. W. *Adv. Polym. Sci.* **1974**, *16*, 1.
(29) Rouse, P. E. *J. Chem. Phys.* **1953**, *21*, 1272.
(30) Schuch, H. *Rheol. Acta* **1988**, *27*, 384.